Optik xxx (2015) xxx–xxx

Contents lists available at ScienceDirect

Optik

journal homepage: www.elsevier.de/ijleo

Thickness dependence on structural, dielectric and AC conduction studies of vacuum evaporated Sr doped $BaTiO_3$ thin films

Sengodan Raja[a], Chandar Shekar Bellan[b,*], Senthilarasu Sundaram[c], Gopal subramani[a], Ranjithkumar Rajamani[d]

[a] Department of Physics, Kumaraguru College of Technology, Coimbatore 641049, Tamil Nadu, India
[b] Departments of Physics, Kongunadu Arts and Science College, G.N-Mills, Coimbatore 641029, Tamil Nadu, India
[c] Environment and Sustainability Institute, University of Exeter, Exeter, UK
[d] Department of Biotechnology, Dr.N.G.P. Arts and Science College, Coimbatore, Tamil Nadu, India

ARTICLE INFO

Article history:
Received 31 August 2015
Accepted 11 December 2015
Available online xxx

Keywords:
Barium strontium titanate
Thermal evaporation
XRD
SEM
TEM

ABSTRACT

Barium titanate ($BaTiO_3$) doped with Strontium (BST) nanoparticles prepared by using wet chemical method were thermally evaporated on to well cleaned glass substrates under the vacuum of 2×10^{-5} Torr, using 12A4 Hind Hivac coating unit. The thickness of the film was measured by quartz crystal monitor. From X-ray analysis, it has been found that $BaTiO_3$ nanoparticles possess tetragonal structure and deposited films has a polycrystalline in nature, whereas the crystallinity of film increases with increase of temperature. Surface morphology of fabricated thin film observed that very homogeneous and uniform size. The transport mechanism in these films under a.c. fields was studied in the frequency range 12 Hz to 100 kHz, at different temperatures (303–483 K). The dependence of dielectric constant and loss factor for different thickness was investigated and results are discussed. The process of a.c. conduction has been explained on the basis of hopping conduction mechanism. The dielectric constant (ε'), temperature co-efficient of capacitance (TCC) and temperature co-efficient of permitivity (TCP) were estimated. The dependences of activation energy on thicknesses also studied and reported.

1. Introduction

Barium titanate doped with strontium having perovskite structure is a common ferroelectric material with a high dielectric constant. It is an attractive material for applications such as multilayer capacitor, pyroelectric detectors, dynamic random access memory device, non-volatile memories, integrated circuit technology, energy storage devices, field-effect transistors, energy harvesters and positive temperature coefficient of resistance [PTCR] sensor [1]. Several novel devices have been fabricated based on Sr doped $BaTiO_3$ thin films, which include phase shifter, thin film capacitors, photovoltaic devices, optoelectronic devices and humidity sensors. Due to the desirable properties and applications, over the last few decades, synthesis of $BaTiO_3$ nanoparticles and thin film has attracted great attention. Most of the experimental work carried out so far relate to preparation of nanoparticles like polymeric precursor method [2] co-precipitation, alkoxide hydrolysis [3], metal-organic processing [4], hydrothermal treatment [5] and the solid state reaction of mixed oxide route [6]. Among this method wet chemical method is a promising technique that offers relative low cost, uniform size and homogenous particles. A detailed survey of the literature reveals that even though some work on dielectric properties has been carried out to prepare thin film of strontium doped barium titanate such as sol–gel method [7,8], r.f. – sputtering [9], pulsed laser ablation [10] and metal-organic chemical vapor deposition [11]. No work is found in the literature about to preparation of thin films by vacuum evaporation method using glass substrate. Hence the present paper discusses the structure, dielectric and a.c. conduction mechanism in vacuum evaporated Sr doped $BaTiO_3$ thin films.

2. Experimental details

2.1. Synthesis of $BaSrTiO_3$ nanoparticles

BST nanoparticles were synthesized using wet chemical method. The starting materials used were barium chloride ($BaCl_2 \cdot 2H_2O$), titanium dioxide (TiO_2), strontium carbonate ($SrCO_3$) and oxalic acid. A solution of Ba:Ti:oxalic acid:$SrCO_3$ having mole ratio 1:1:1:0.1 was stirred and evaporated at 70 °C till a clear, viscous resin was obtained and then dried at 110 °C for 20 h. The

* Corresponding author. Tel.: +91 8526182494.
E-mail address: chandar.bellan@gmail.com (C.S. Bellan).

http://dx.doi.org/10.1016/j.ijleo.2015.12.072
0030-4026/

precursor formed was heated at 900 °C for 2 h to form BST nanoparticles. So the chemical composition of our BST nanoparticles is follows

$BST = BaSr_{0.1}TiO_3$.

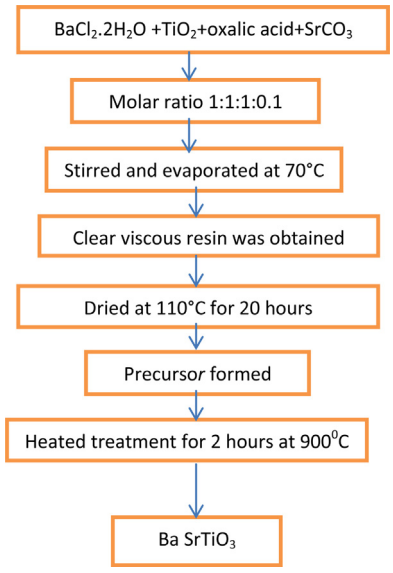

2.2. $BaTiO_3$ thin film preparation

Using the conventional 12A4 Hind Hivac coating unit, pure (99.999%) aluminium was evaporated from a tungsten filament onto well-cleaned glass substrates through suitable masks to form the bottom electrode. Prepared BST nanoparticles were then evaporated from a molybdenum boat to form the dielectric layer. An aluminium counter electrode was evaporated onto the dielectric through suitable masks to complete the aluminium–$BaTiO_3$–aluminium (metal–insulator–metal structure) device. A working pressure of 2×10^{-5} Torr was maintained in all the evaporation processes. For the structural analysis, the BST films were deposited on the plane glass substrates.

2.3. Measurements

Thickness of the films was measured through quartz crystal monitor ("Hind Hivac" Digital Thickness Monitor Model–DTM–101). The structural aspects of the films were analyzed, using X-ray diffractometer with filtered Cu$K\alpha$ radiation ($\lambda = 1.5418$ Å). The surface morphology BST was examined by scanning electron microscope (SEM) and the high-resolution transmission electron microscopy (HRTEM). Measurements of series capacitance and the dissipation factor in the frequency range 12 Hz–100 kHz were carried out at various temperatures (303–483 K) using digital LCR meter (LCR-819, GW instek, Good will Instrument company Ltd., Taiwan). The dielectric constant ε' was evaluated from the capacitance data from the known area and thickness of the dielectric films.

3. Result and discussion

3.1. EDS analysis

Figs. 1 and 2a–c show the EDS spectrum of as prepared $BaTiO_3$ nanoparticles and as deposited $BaTiO_3$ thin film of various thicknesses. Elemental composition analysis indicated the presence of Ba, Ti, Sr and O in the synthesized $BaTiO_3$nanoparticles as well as in the $BaTiO_3$ thin films

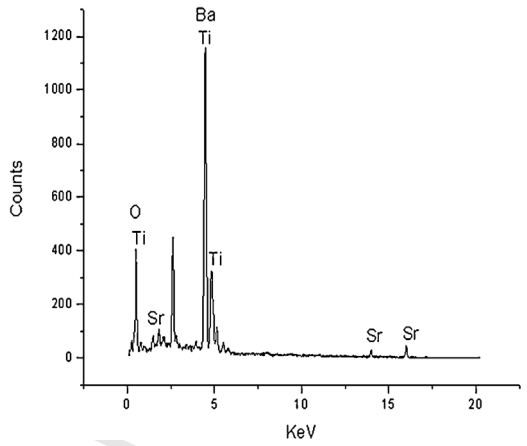

Fig. 1. EDS spectrum of the BST nanoparticles.

3.2. Surface morphology

3.2.1. Scanning electron microscope (SEM) studies

Fig. 3 shows the SEM images of BST particles. Rod like and uniform grain size are distributed throughout the particles. Fig. 4a–c shows the SEM images of the BST thin films at different thickness. In all the films micro cracks were observed. These are attributed to the volume contraction during the crystallization process and the stress caused by the mismatch in thermal expansion coefficient between the film and substrate [12]. The grain size of the films increases with increasing thickness, it could be attributed to higher grain growth at higher thickness [13].

3.2.2. Transmission electron microscope (TEM)

Fig. 5a shows the HRTEM micrography of the BST nanoparticles with a well-isolated rod like morphology. The diameter of the rod is around 50–70 nm. Fig. 5b is the SAED pattern of the nanorods, which reveals that the BST products exhibit a tetragonal structure

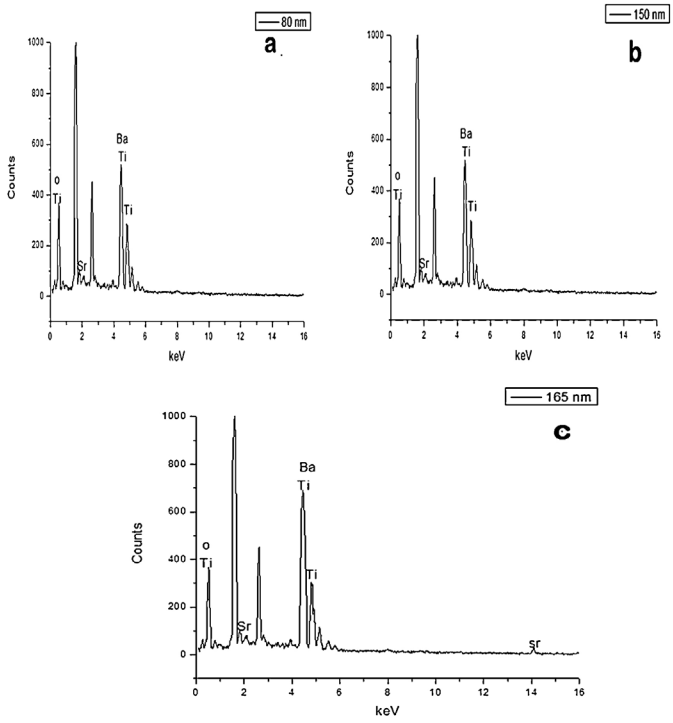

Fig. 2. EDS spectrum of the $BaTiO_3$ thin films (a) 80 nm, (b) 150 nm and (c) 165 nm.

Please cite this article in press as: S. Raja, et al., Thickness dependence on structural, dielectric and AC conduction studies of vacuum evaporated Sr doped $BaTiO_3$ thin films, Optik - Int. J. Light Electron Opt. (2015), http://dx.doi.org/10.1016/j.ijleo.2015.12.072

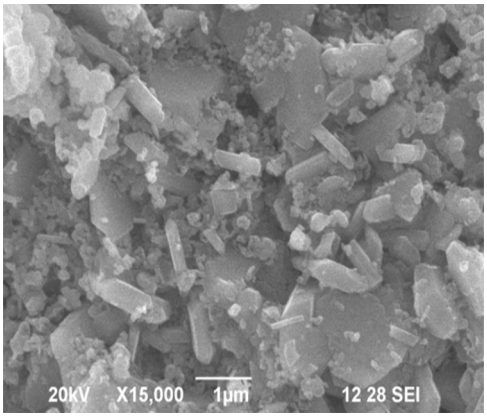

Fig. 3. SEM image BST nanoparticles.

[14]. Fig. 5c shows the fringing spacing of the nanorod. According to the image, well-resolved lattice fringes can be seen clearly, which give further information on fine micro-structure of the rod like BST nanoparticles. The fringe spacing of 2.857 Å corresponds to the (1 1 0) planes of nanoparticles.

3.3. X-ray diffraction analysis

Fig. 6 shows the XRD pattern of BST nanoparticles. From XRD measurement, the BST particle is exhibited to the tetragonal structure, because the peak splitting was found clearly in the (0 0 2) plane, which shows its high degree of tetragonality [15,16]. The average grain size (D) of the particle was calculated using scherrer's formula and it was found to be 66 nm.

The crystallite size is calculated from the Scherrer's formula from the full with half–maximum (FWHM) of the XRD peaks

$$D = \frac{0.94\lambda}{\beta \cos\theta} \quad (1)$$

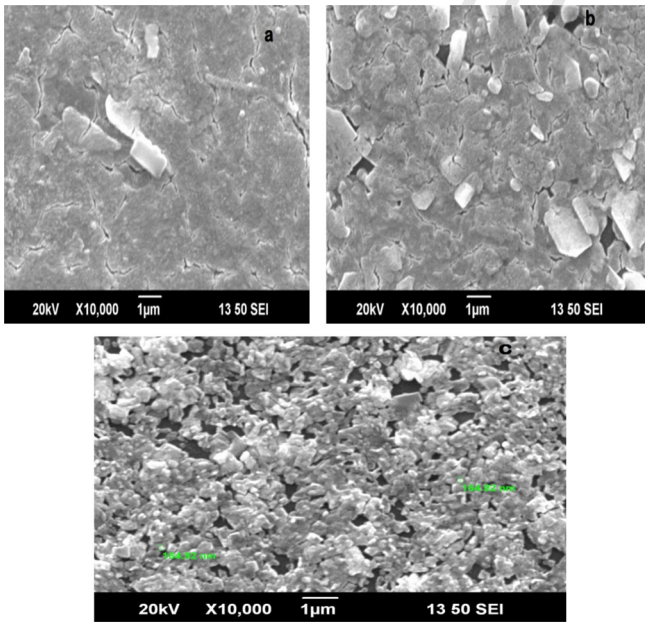

Fig. 4. SEM image $BaTiO_3$ thin films (a) 80 nm, (b) 150 nm and (c) 165 nm.

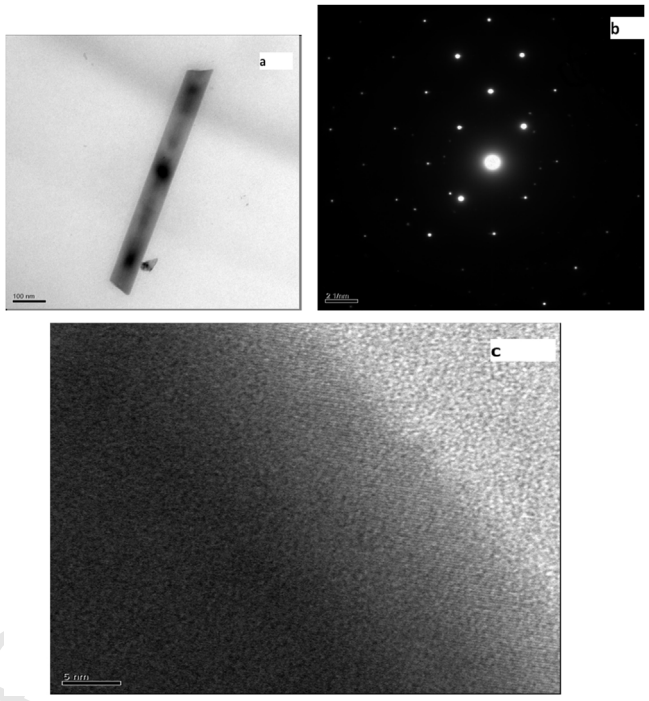

Fig. 5. TEM images of BST nanoparticles (a) nanorod, (b) SAED pattern and (c) the fringing spacing.

where λ is the wavelength of the X-rays used, 2θ is the angle between the incident and scattered X-rays and β is the full width at half maximum. The strain (ε) is calculated from the formula

$$\varepsilon = \frac{\beta \cos\theta}{4} \quad (2)$$

The dislocation density (δ) is defined as the length of dislocation lines per unit volume of the crystal and is given by

$$\delta = \frac{1}{D2} \quad (3)$$

Fig. 7 shows the XRD patterns of the BST thin films deposited on glass substrate with different film thickness. The films were found to be polycrystalline with (0 0 1) (1 1 0), (1 1 1), (2 0 0),(1 0 2) and (1 1 2) peaks arising at 2θ values of 23.95°, 30.30°, 36.84°, 43.06°, 52.64° and 56.63°, respectively. The intensity of (1 1 0) peak was higher than (1 1 1) and (2 0 0) peaks. As can be seen, the crystallization of the films strongly depends on the film thickness. The intensity of the peak increases with increase in film thickness, indicating good crystallinity [17].

Table 1 shows the calculated values of crystalline size (D), dislocation density (δ) and strain (ε) for different thickness. From the table it has been observed that the grain size increases with increase

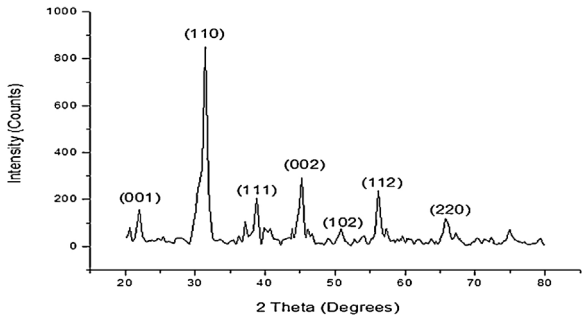

Fig. 6. XRD pattern of BST nanoparticles.

Please cite this article in press as: S. Raja, et al., Thickness dependence on structural, dielectric and AC conduction studies of vacuum evaporated Sr doped $BaTiO_3$ thin films, Optik - Int. J. Light Electron Opt. (2015), http://dx.doi.org/10.1016/j.ijleo.2015.12.072

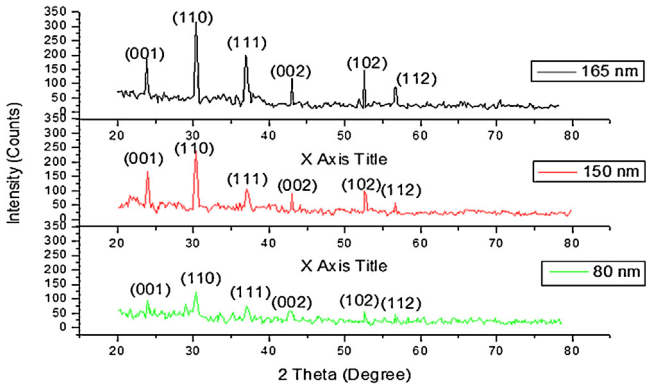

Fig. 7. XRD pattern of BST thin films for different thickness.

Table 1
Structural parameters of BST thin films of different thicknesses.

Thickness (nm)	D (nm)	$\delta \times 10^{15}$ (lin m^{-2})	$\varepsilon \times 10^{-3}$ (lin^{-2} m^{-4})
80	28.32	2.2059	1.5037
150	44.44	0.825	0.917
165	51.55	0.491	0.7383

in thickness whereas the strain and the dislocation density decrease with the increase in thickness. Due to the increase in grain size with film thickness, the defects in the lattice are decreased, which in turn reduce the internal micro strain and dislocation density/or the columnar grain growth is increased [18].

3.4. Dielectric studies

The capacitance, dielectric constant and dielectric loss are important parameter in the selection of materials for device application. The dielectric constant (ε_r) is evaluated from the equation.

$$\varepsilon_r = \frac{Cd}{\varepsilon_0 A}$$

where C is the capacitance, d is the thickness of the dielectric, ε_0 is the permittivity of free space and A is the area of the dielectric.

3.4.1. Frequency effect

Fig. 8 shows the variation of dielectric constant with frequency for various thicknesses at room temperature of BST thin films. The dielectric constant increases with increase in film thickness whereas the dielectric constant decreases with increase in frequency. The observed decrease of dielectric constant with

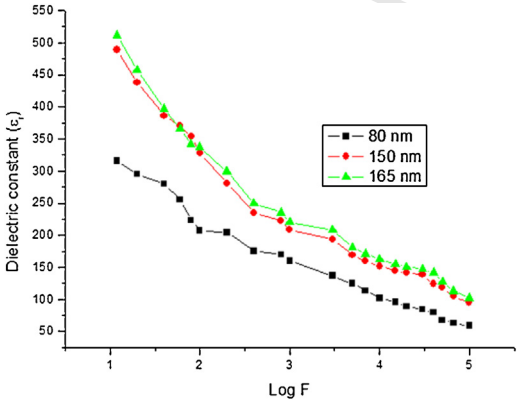

Fig. 8. The variation of dielectric constant with frequency for various thicknesses at room temperature of BST thin films.

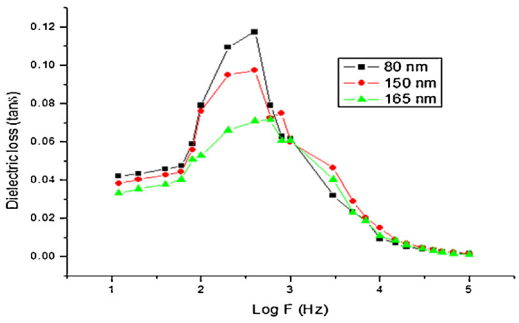

Fig. 9. Variation of tan δ with frequency for various film thicknesses at room temperature of BST thin films

increasing frequency may be due to the tendency of induced dipoles to orient themselves in the direction of the applied field. The following equation can explain the observed dependence of dielectric constant $\varepsilon(\omega)$ with frequency [19].

$$\varepsilon(\omega) = \frac{\varepsilon''(\omega)}{\tan\delta} = \frac{\varepsilon''(\omega)}{(1/\omega RC + \omega RC)}$$

where the value of $\varepsilon(\omega) \alpha 1/\omega RC$ at low frequency and $\varepsilon(\omega) \alpha \omega RC$ at higher frequency.

When $\omega = 0$, $\varepsilon''(\omega) \approx 0$ then $\varepsilon(\omega) = \varepsilon_s$ (static dielectric constant) and when ω (œ), $\varepsilon''(\omega) \approx \infty$ then $\varepsilon(\omega) = \varepsilon_{œ}$ (dielectric constant at optical frequency). The observed dielectric spectrum shows the weak polar nature of the BST films. In vacuum evaporated thin films, the growth processes produce agglomeration and hence porosity formed in thin films. As the thickness of the film increases, the density of voids decreases and hence the dielectric constant increases. Fig. 9 shows the typical variation of tan δ with frequency for various film thicknesses at room temperature of BST thin films. The loss factor is found to increase with increasing frequency in all thickness up to the frequency 1 kHz. The appearance of peak in tan δ near 1 kHz and 800 Hz frequencies suggests the existence of resonance frequencies. At resonance frequencies the dielectric losses become maximum [20]. Further, the decrease of tan δ with increase in frequency after maximum tan δ value can be explained by Debye formula [21]. According to this formula tan δ is inversely proportional to frequency which explains the decrease in tan δ with the increase in frequency beyond maximum tan δ.

3.4.2. Temperature effect

Temperature dependencies of the capacitance at the frequency of 1 kHz for different thicknesses are displayed in Fig. 10. It has been observed that the capacitance decreases with increase in thickness whereas capacitance increases with increase temperature and it attains its maximum value at Curie temperature (T_c)

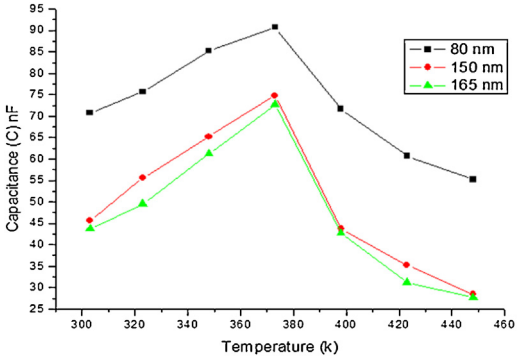

Fig. 10. Temperature dependencies of the capacitance at the frequency of 1 kHz for different thicknesses.

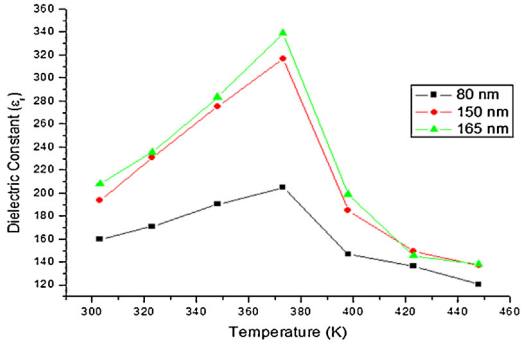

Fig. 11. Temperature dependencies of the dielectric constant at the frequency of 1 kHz for different thicknesses.

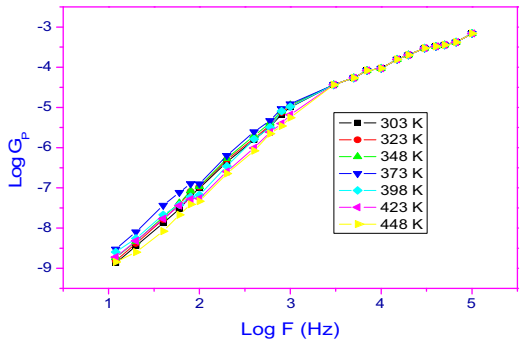

Fig. 12. The dependence of AC conduction on frequency at different temperatures for the Sr doped $BaTiO_3$ thin film of thickness 165 nm.

378 K and above T_c it decreases indicating that phase transition from ferroelectric to paraelectric phase. The temperature coefficient of capacitance (TCC) is an important parameter for assessing the expected behavior of thin film circuits.

The temperature coefficient of capacitance has been evaluated using the relation.

$$\mathrm{TCC} = \gamma_c = \frac{1}{\left((C\,\mathrm{d}C)/\mathrm{d}T\right)}$$

Temperature dependencies of the dielectric constant at the frequency of 1 kHz for different thicknesses are displayed in Fig. 11. The dielectric constant increases with increase in thickness and temperature up to the Curie temperature (T_c) 373 K and above T_c it decreases indicating phase transition from ferroelectric to paraelectric phase. The shift in the Curie temperature is lower than the pure $BaTiO_3$ thin film. Several other have also reported a shift in the $BaTiO_3$ Curie temperature with wide limits, depending on the average grain size, in homogeneities, internal stresses and sintering temperature [22–24] Table 2 shows the estimated TCC and TCP values for the films of different thicknesses at a frequency of 1 kHz. It is found that the TCC and TCP values increase with increase in thickness. The low values of TCC and TCP of the material suggest its suitability for capacitor applications.

3.4.3. AC conduction

The dependence of AC conduction on frequency at different temperatures for the Sr doped $BaTiO_3$ thin film of thickness 165 nm is shown in Fig. 12. The AC conductance has been found to vary according to the relation $Gp\,\alpha\,f^n$, where the value of n depends on the temperature and frequency. The curves exhibit two dispersion regions one below 400 Hz and the other above 400 Hz. At room temperature n values range from 0.96 to 1.4. In the second region (>400 Hz), nearly all the curves approximate to a square law dependence on frequency and show less dependence on temperature at higher frequencies [25]. This behavior reveals that the mechanism for AC conduction is hopping of charge carriers.

Fig. 13 exhibits the thickness dependence of conductance for different thickness at 1 kHz and the estimated activation energy is presented in Table 3. As seen in the table, the activation energy decreases as the thickness increases. The observed low value of activation energy suggests that the conduction mechanism in these films may be due to the hopping of electrons.

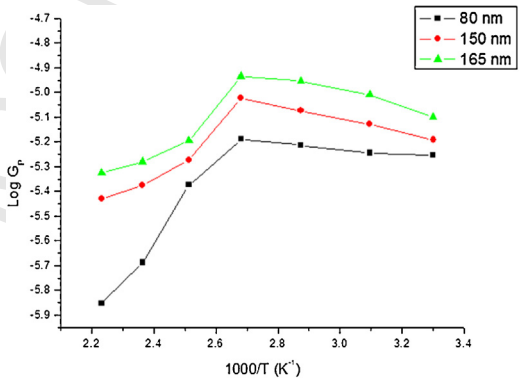

Fig. 13. Thickness dependence of conductance for different thickness at 1 kHz.

Table 2
Thickness dependence of TCC and TCP values of BST film at 1 kHz.

Thickness (nm)	TCC (ppm/k)	TCP (ppm/k)
80	4215	4370
150	8933	7526
165	9631	8436

Table 3
Activation energy dependence on thickness.

Thickness (nm)	Activation energy (eV)
80	0.3240
150	0.2455
165	0.2374

4. Conclusion

We have successfully synthesized nanoparticles of Sr doped $BaTiO_3$ by low cost of wet chemical method using commercially available chemicals such as $BaCl_2$, TiO_2, $SrCO_3$ and oxalic acid. Thin films of few hundred nanometer thickness was prepared on well cleaned glass plate for the first time using thermal evaporation method. X-ray analysis showed that particle has a tetragonal nature and the deposited film has a polycrystalline nature, whereas crystallinity increases with increase in thickness. The dielectric constant of the film increases with increase in thickness. In the low frequencies and at higher temperatures, the capacitance is dependent both on temperature and frequency whereas it is independent of frequency at low temperature and high frequencies. But the dielectric constant and loss factor always shows a dependence on frequency and thicknesses. The low value of TCC and TCP of the material are suitable for capacitor applications. The a.c. conduction mechanism in the films has been explained on the basis of hopping of charge carriers. The activation energy is found to be thicknesses dependent and it is also observed that decreases with increase of thicknesses.

References

[1] R. Sengodan, B. Chandar Shekar, S. Sathish, Structural and optical properties of nano scale $BaTiO_3$ thin films prepared from $BaTiO_3$ nanoparticles synthesised

Please cite this article in press as: S. Raja, et al., Thickness dependence on structural, dielectric and AC conduction studies of vacuum evaporated Sr doped $BaTiO_3$ thin films, Optik - Int. J. Light Electron Opt. (2015), http://dx.doi.org/10.1016/j.ijleo.2015.12.072

by organic acid precursor method, J. Optoelectron. Adv. Mater. 14 (2012) 653–657.
[2] V. Vinothini, Paramanard Singh, M. Balasubramanian, Synthesis of barium titanate nanopowder using polymeric precursor method, Ceram. Int. 32 (2006) 99.
[3] K.W. Kirby, Alkoxide synthesis techniques for $BaTiO_3$, Mater. Res. Bull. 12 (1988) 881.
[4] A.S. Shaikh, G.M. Vest, Kinematics of $BaTiO_3$ and $PbTiO_3$ formation from metallo–organic precursors, J. Am. Ceram. Soc. 69 (1986) 682.
[5] M. Boulos, S. Fritsch, F. Mathieu, B. Durand, T. Lebey, V. Bley, Hydrothermal synthesis of nanosized $BaTiO_3$ powders and dielectric properties of corresponding ceramics, Solid State Ionics 176 (2005) 1301.
[6] A. Beauser, J.C. Niepce, Role and behaviour of orthotitanate Ba_2TiO_4 during the processing of $BaTiO_3$ based ferroelectric ceramics, J. Mater. Sci. 19 (1984) 195.
[7] L.V. Maneeshya, V.S. Anitha, Sujatha S. Lekshmy, I. John Berlin Prabitha, B. Nair Georgi, P. Daniel, P.V. Thomas, K. Joy, Influence of annealing temperature and oxygen atmosphere on the optical photoluminescence properties of $BaTiO_3$ amorphous thin films prepared by sol–gel method, J. Mater. Sci.: Mater. Electron. 24 (2013) 848–854.
[8] Z. Hu, G. Wang, Z. Huang, X. Meng, J. Chu, Investigation on the infrared optical properties of $BaTiO_3$ ferroelectric thin films by spectroscopic ellipsometry, Semicond. Sci. Technol. 18 (2003) 449.
[9] P. Bhattacharya, T. Komeda, D. Park, Y. Nishioka, Comparative study of amorphous and crystalline (Ba, Sr) TiO_3 thin films deposited by laser ablation, Jpn. J. Appl. Phys. 32 (1993) 4103.
[10] S.G. Yoon, J. Lee, A. Safari, Characterization of $(Ba_{0.5},Sr_{0.5})TiO_3$ thin films by the laser–ablation technique and their electrical properties with different electrodes, Integr. Ferroelectr. 7 (1995) 329.
[11] D. Tahan, A. Safari, L.C. Klin, Sol–gel synthesis of barium strontium titanate thin films for capacitor applications, J. Am. Ceram. Soc. 79 (1996) 1593.
[12] C.B. Samantaray, A. Dhar, D. Bhattacharya, M.L. Mukherjee, S.K. Ray, Effect of post-deposition annealing on microstructural and optical properties of barium strontium titanate thin films deposited by r.f. magnetron sputtering, J. Mater. Sci.: Mater. Electron. 12 (2001) 365–370.
[13] Raja Sengodan, Bellan Chandar Shekar, Sugumaran Sathish, Structural and DC conduction studies on vacuum evaporated $BaTiO_3$ thin films prepared from $BaTiO_3$ nano particles synthesised by wet chemical method, Optik 125 (2014) 4819–4824.
[14] R. Sengodan, B. Chandar Shekar, Characterization of barium strontium titanate single crystal nanorods prepared by wet chemical method, J. Optoelectron. Adv. Mater–Rapid Commun. 8 (2014) 617–621.
[15] Bruce.D. Begg, Eric.R. Vance, Janusz Nowotny, Effects of particle size on the room temperature crystal structure of $BaTiO_3$, J. Am. Ceram. Soc. 77 (1994) 3186–3192.
[16] B.D. Stojannovic, A.Z. Simoes, C.O. Paiva-Santos, Mechanochemical synthesis of barium titanate, J. Eur. Ceram. Soc. 25 (2005) 1985–1989.
[17] S. Kribalis, P.E. Tsakiridis, C. Dedeloudis, E. Hristoforou, Structural and electrical characterization of barium strontium titanate films prepared by sol–gel technique on brass (CuZn) substrate, J. Optoelectron. Adv. Matter. 8 (2006) 1475–1478.
[18] M. Sridharan, Sa.K. Narayandass, D. Mangalaraj, H.C. Lee, Characterization of vacuum evaporated polycrystalline $Cd_{0.96}Zn_{0.04}Te$ thin films by XRD, Raman scattering and spectroscopic ellipsometry, Cryst. Res. Technol. 37 (2002) 964.
[19] R. Sengodan, B. Chandar Shekar, S. Sathish, Morphology, structural and dielectric properties of vacuum evaporated V_2O_5 thin films, Phys. Procedia 49 (2013) 152.
[20] D.J. Griffiths, Introduction to Electrodynamics, third ed., Prentice Hall, India, 1998.
[21] A.K. Singh, T.C. Goel, R.G. Mendiratta, O.P. Jhakur, C. Prakash, Dielectric properties of Mn-substituted Ni–Zn ferrites, J. Appl. Phys. 91 (2002) 6626.
[22] R. Sengodan, B. Chandar Shekar, S. Sathish, Structural, dielectric and AC conduction studies on vacuum evaporated $BaTiO_3$ nano thin films prepared from $BaTiO_3$ nano particles, J. Nanoelectron. Optoelectron. 8 (2013) 1–6.
[23] G. Arlt, D. Hennings, G. Dewith, Dielectric properties of fine—grained barium titanate ceramics, J. Appl. Phys. 58 (1985) 1619–1625.
[24] T. Yoko, K. Kamiya, K. Tanaka, Preparation of multiple oxide $BaTiO_3$ fibers and the sol–gel method, J. Matter. Sci. 25 (1989) 3922.
[25] P. Matheswaran, R. Sathyamoorthy, R. Saravanakumar, S. Velumani, AC and dielectric properties of vacuum evaporated InTe bilayer thin films, Mater. Sci. Eng., B. 174 (2010) 269–272.

Please cite this article in press as: S. Raja, et al., Thickness dependence on structural, dielectric and AC conduction studies of vacuum evaporated Sr doped $BaTiO_3$ thin films, Optik - Int. J. Light Electron Opt. (2015), http://dx.doi.org/10.1016/j.ijleo.2015.12.072